



A Plasma Arc-Based Electromechanical System Designed for Microchannel Processing

Fevzi Akın¹ · Ece Ersoy¹ · Deniz İdil² · Melih Özsimiççi¹ · Dilek Çökeliler Serdaroğlu¹ · Yusuf Tansel İç² · Kumru Didem Atalay² · Cengiz Koçum¹ · Kemal Okat²

Received: 22 December 2023 / Accepted: 25 April 2024 / Published online: 19 May 2024
© The Author(s) 2024

Abstract

Plasma technology is based on a simple physical principle. When more energy enters the gas, it ionizes and becomes the fourth state of matter, the energy-dense plasma. The studies carried out within the scope of this study were designed to create microchannels on lamellar glass using an improved redesign of the current plasma arc device, which is the main subject of the paper. The created microchannel is examined at the microscale. Experimental analysis was conducted considering the effect of plasma on the effect of microchannel quality. We performed an experimental design study to determine the optimal parameter levels for improving microchannel quality. The predicted results have been validated with the experimental results. An experimental design study provides useful results, such as information about the distance between the probes, pulse duration, and material temperature, which enhances the channel dimensions. The improved device can be utilized effectively to establish microchannel processing in practice.

Keywords Microchannel · Plasma arc device · Plasma arc drilling · Experimental design · Production design

1 Introduction

Microchannel processing on transparent workpieces using plasma is a complex process. Microchannels are used in crucial and critical processes in the medical and optical equipment industries. Today, the use of microfluidic-based chips in personalized and clinical diagnostic operations is becoming widespread [1]. Such technologies include electrochemical biomedical devices, optical and fiber optic sensors, biosensors, and microfluidic technology. Essentially, these technologies require materials with high impact strength, high dimensional and chemical stability, high transparency, and optical clarity. Therefore, the demand for industrial processing of transparent materials is increasing. Materials such as polycarbonate (PC) [2, 3], polyimide (PI) [2], polydimethylsiloxane (PDMS) [4], glass [5], and polymethyl methacrylate (PMMA) [6, 7] are the most common transparent materials used in the manufacture of biomedical equipment. On the other hand, glass is one of the most widely used transparent materials for biomedical equipment. Glass is a crucial material, and its eco-friendliness, dimensional stability, and inherent toughness make it an ideal material in the medical equipment industry.

✉ Yusuf Tansel İç
yustanic@baskent.edu.tr

Fevzi Akın
fevziakin1996@gmail.com

Ece Ersoy
ecersoy2000@hotmail.com

Deniz İdil
idild Deniz2000@gmail.com

Melih Özsimiççi
melihcazz@hotmail.com

Dilek Çökeliler Serdaroğlu
cokeliler@baskent.edu.tr

Kumru Didem Atalay
katalay@baskent.edu.tr

Cengiz Koçum
kocum@baskent.edu.tr

Kemal Okat
21594699@mail.baskent.edu.tr

¹ Department of Biomedical Engineering, Baskent University, 06790 Ankara, Turkey

² Department of Industrial Engineering, Baskent University, 06790 Ankara, Turkey



In the current sensing plasma arc device mentioned in the study, performing the microchannel process by turning air into plasma is an unusual manufacturing method. Plasma, which is a tool for performing microchannel fabrication, is the fourth state of matter. Plasma also contains ionized gas. A high temperature, high voltage, or high pressure can also cause this to occur. At the end of the study, necessary corrections were made to the current sensing plasma arc device, and microchannel processing was improved by determining the factors related to the process and determining which factor levels produced the best results. A microchannel profile was produced on a substrate (glass and quartz-like) by the plasma arc method. Our goal was to produce a smooth microchannel.

According to the results of the literature survey, micro-hole drilling methods are widely used. However, if we look at microchannel processes with plasma, studies on this subject are not as common as other methods. Drilling methods investigated within the scope of the literature review included drilling with electrochemicals, electrolytic drilling with a shaped pipe, electron beam drilling, drilling with electrodischarge, photochemical drilling, capillary drilling, drilling with a jet electrolytic, laser drilling, drilling with electroflow, ultrasonic drilling, and plasma arc drilling [8–10].

Since there is no method based on the working principle of the current sensing plasma arc device in these studies, the method of constructing a microchannel with a plasma arc, which has a working principle similar to the working principle of this method, has been discussed. The short duration of the process, the continuous formation of the channel, and the ability to work on surfaces that are more difficult to drill than other methods are indicators of the increase in use of the plasma arc method. While determining the parameters of the plasma arc microchannel method, the parameters of the hole drilling methods used in the experiments examined in the literature review were taken into account. The parameters used according to the articles are shown in Table 1.

A literature survey illustrates that the plasma drilling operation is widely used in manufacturing processes. However, the plasma microchannel processing operation and its stability have not been investigated in detail. Therefore, it is necessary to obtain the process parameters and the corresponding range of optimal stability of the system to fill this research gap. Therefore, the main motivation of this paper is to propose optimal processing conditions for microscale plasma microchannels.

1.1 Current Device Specifications

When every substance is in the gas phase, when it is heated to a temperature that varies depending on its type, property, and nature, the atoms lose their outer shell electrons due to the movement of their molecules, which turn them into positively charged ions. Figure 1 shows the plasma source. As the

Table 1 Literature summary

Ref	Year	Hole depth	Power	Current	Hole diameter	Cutting speed	Hole tolerance	Gas type	Torch height	Work-pat height	Frequency	Material type	Manufacturing lead time	Impact energy	Torch angle
[11]	2005	X	X		X		X					X			X
[12]	2011		X	X		X		X	X			X			
[13]	2010					X						X	X		
[14]	2011			X		X			X	X		X	X		
[15]	2010			X		X			X	X		X	X		
[16]	2022			X		X			X						
[17]	2003		X		X									X	
[18]	1996		X												
[19]	2002		X		X										
[20]	1986		X	X		X					X				X
[21]	2013		X			X					X				
[22]	1996			X				X							
[23]	2018			X											X
[24]	2014			X											X



Fig. 1 Plasma beam formation in a plasma arc device

temperature increases, the degree of ionization, that is, the percentage of the total number of ionized atoms, increases. After a threshold value changes depending on the substance, such as a few tens of thousands of degrees, there is only a mixture of positively charged ions and negatively charged free electrons in the environment. This mixture, which is electrically neutral and conductive because it consists of charged particles, is called “plasma” [3].

The steps to produce a microchannel by the plasma arc method are as follows:

STEP 1: The device is plugged into the socket. The Arduino is connected to the computer, and the code works in this way.

STEP 2: The distance between the probes. In addition, the alignment of the probes was performed. The two probes were aligned with each other to the same extent.

STEP 3: The mechanism we designed on the glass device on which the channel will be formed is placed. The glass placed in this way remains between the two probes, and the distance of the glass to the two probes is the same. In other words, the glass is placed in the middle of the two probes.

STEP 4: The first step in the channel is to create a hole in the glass. Shooting was performed on the button of the device, and the device was left for 3 s. After 3 s, the hole was opened.

STEP 5: The drilled hole is accepted as the starting point of the channel. Starting from this hole, the system is moved. When the required distance is reached, another hole is created. After each shot, the plate was left for approximately 1 s. When it waits for more than 1 s, the glass cracks.

STEP 6: A channel is created by drilling holes side by side.

The current sensing plasma arc device, patented by Baskent University faculty members, is controlled by a computer. Figure 2 shows the plasma arc device. A schematic of

the device is shown in Fig. 3. The device starts to work by pressing the button connected to the device according to the frequency, power, and operation time, which can be adjusted via the code. The device performs the hole drilling process by providing air conductivity with high voltage and creating plasma, which is the fourth state of matter.

Two tungsten tips, which are made up of parts of the device, form a resonant circuit between the material to be drilled and the remaining system placed between the tips. The plasma gas, which becomes ionized and electrically conductive upon reaching a very high temperature, is transferred to the material from the tungsten tips. The heat of the plasma gas formed here melts the material. As the material melts, a hole is formed.

At the time the device was first used, it was working manually. The frequency, power, and processing time of the device, which started to work when the button was pressed, could not be adjusted practically, causing inefficiency in the work done. To prevent this situation, the device was computer aided by using up-to-date technology, and lower and upper limits were determined with the established algorithm, allowing desired changes in current, power, and operation time to be made possible. Thus, numerous experimental possibilities are presented, which are very easy to see and compare. While working with the device, if another factor is added and desired to work, additions can be made to the algorithm.

2 Improvement of the Existing Device

The lamellar glass was moved manually while the grooving operations were carried out in the existing device. We canceled this manual operation and turned it into a fully automatic system with the help of a stepper motor. While designing this system, a frame is formed by taking the measurements of the device and estimating the sigma profiles (Fig. 4). Linear rails are adapted to the device framework. A slot was created on the carrier panel (work table) where we could place the glass. A section is formed in the lower part of the carrier panel where the ball-screw shaft can enter. The ball-screw shaft integrated into the stepper motor is attached to this area, and movement is provided. The control of the stepper motor is provided by the Arduino code.

Numerical control is preferred for faster production and higher accuracy because of better control over crucial process variables such as standoff distance and feed rate [8]. Hong et al. [25] stated that the vibrations generated during the plasma arc-based manufacturing process impact the sensitivity of the system. The position or size of the arc can be controlled in real time to reduce the sensitivity of the system and maintain it within a reasonable range.

Hong et al. [25] offered a future scope for the unique value of system stability. These authors preliminarily determined

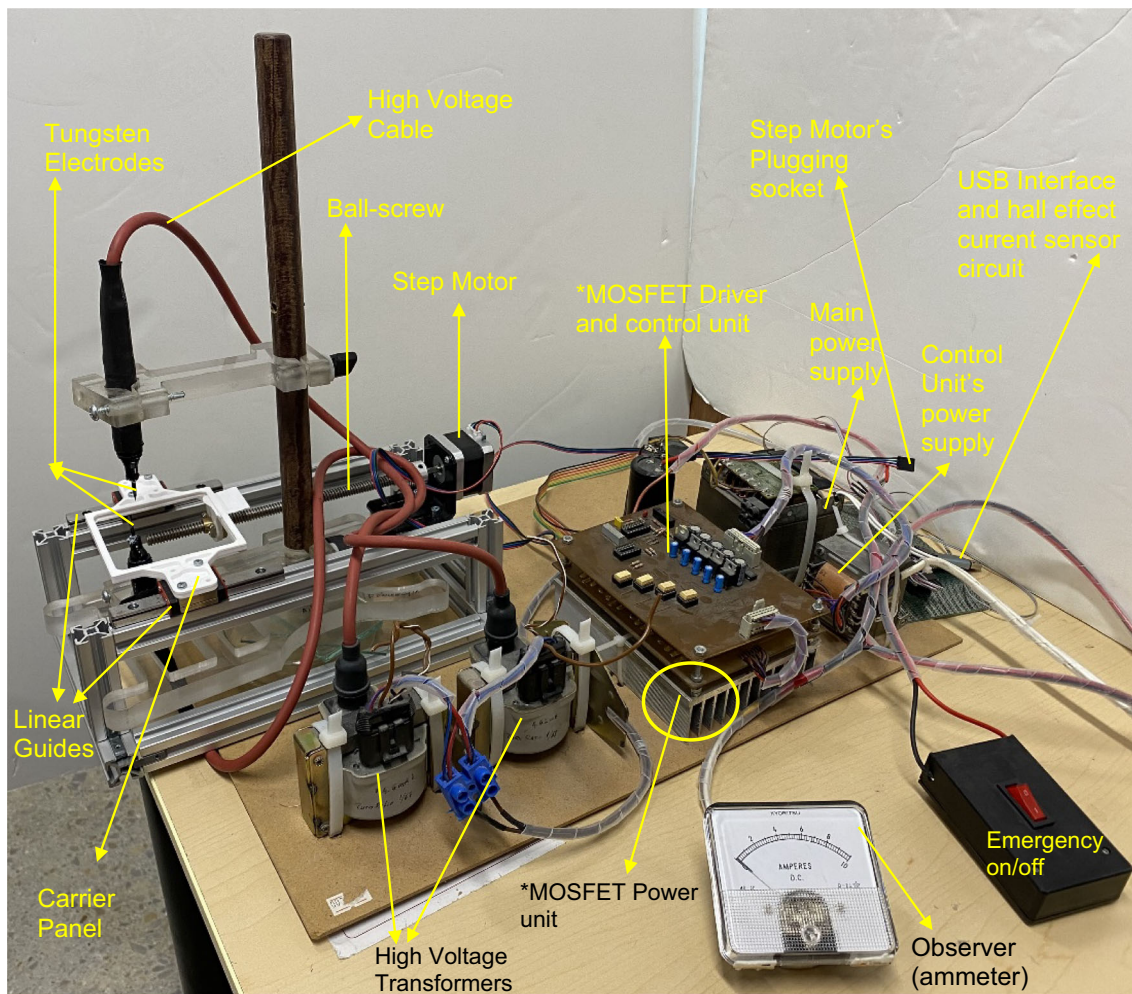


Fig. 2 The plasma arc device and its components. *MOSFET: Metal–Oxide–Semiconductor Field-Effect Transistor

the stability coefficient of the plasma arc welding (PAW) process. They suggested that it is necessary to determine the process parameters and the corresponding range of optimal stability of the system. It is suitable for use in both step motor-driven systems and manual bearing systems. In terms of balance, the linear guide is selected according to the material dimensions and load values to be transported. In addition, more efficient results are obtained if the rail dimensions are determined according to the moment direction and values. The stepper motors used are two-phase motors. The system is operated by providing the necessary commands to a stepper motor driver suitable for the characteristics of the stepper motor. A TB6600 stepper motor driver control board can output up to 4 Amps. Interference and fluctuations are minimized with high-speed optocoupler isolated signal input, and heating problems are minimized with its large heatsink. Up to 32 segments can be used with six selectable modes. It has

built-in overheating, overcurrent, and reverse voltage protection. The features of the step motor used in our system are as follows:

Model: 17HS3401,

Step angle: 1.8° ,

Motor length: 40 mm; operating current: 1.7 A; internal resistance: 1.5Ω .

Phase inductance: 2.8 mH,

Holding torque: 35 Ncm,

Trigger torque: 2.2 Ncm,

Rotor inertia: 54 gcm^2 ,

Weight: 280 g.

Our four-wire step motor has two phases, and there are two wires for each phase. We distinguished this with color codes. In the connection phase, we connected the wires that made up each phase to the relevant pins of the driver according to the labels indicating the phases on our driver (A +, A-, B +, B-). We connected the two wires forming phase A to pins A + and A- and the wires forming phase B to pins B + and B-. We

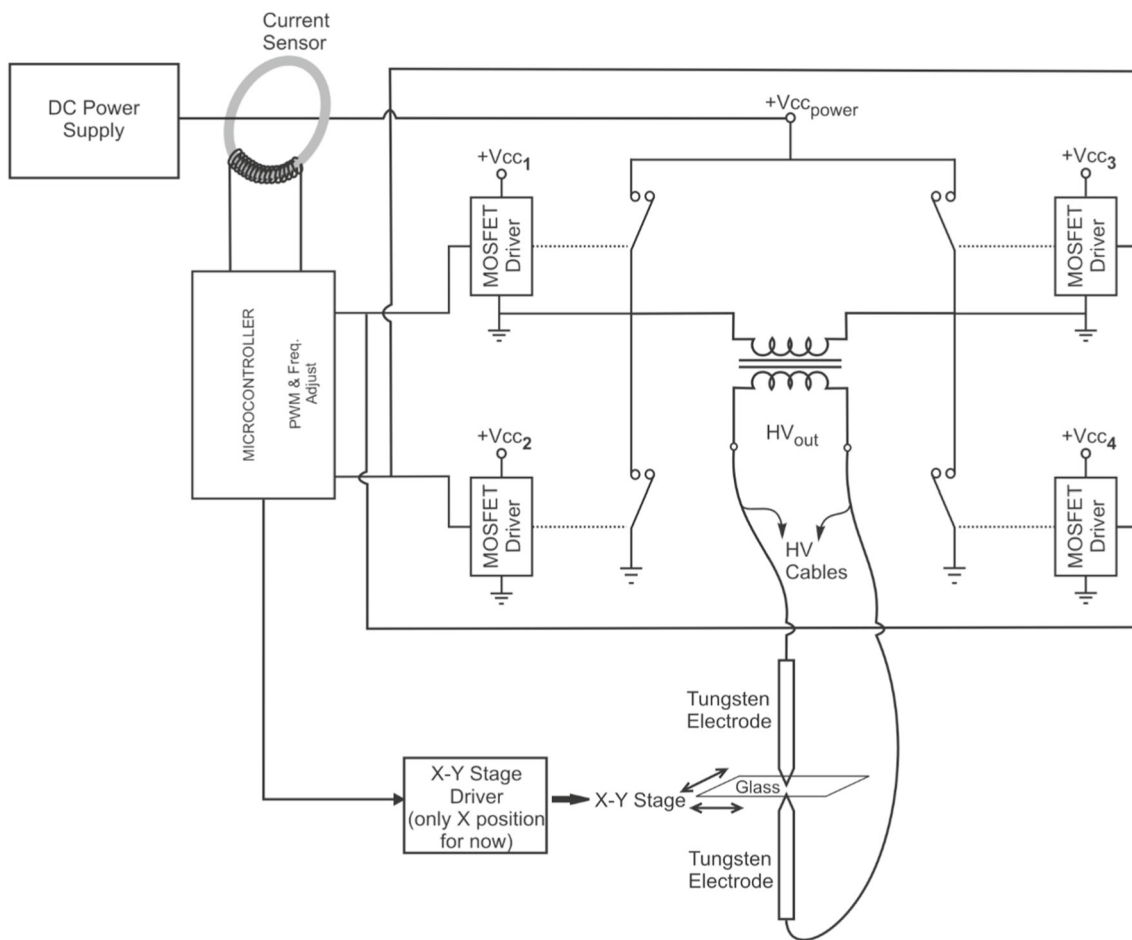


Fig. 3 Schema for the current plasma arc device

connected the driver to the power supply. We tested whether the driver satisfied the voltage and current requirements and tested the action of the stepper motor (Fig. 5).

We use the Arduino Code to run the step motor as follows:

```

Begin;
    Define step motor connections and steps per revolution;
    Set the spinning direction clockwise;
    Set the spinning direction counterclockwise;
    Spin the stepper motor 5 revolutions fast;
    Set the spinning direction counterclockwise;
    Spin the stepper motor 5 revolutions fast;
End.
    
```

2.1 Carrier Panel Design

The carrier panel is designed to make the car a single chassis because of the slot on it. The system also serves to place the glasses and moves the carrier panel by means of a stepper

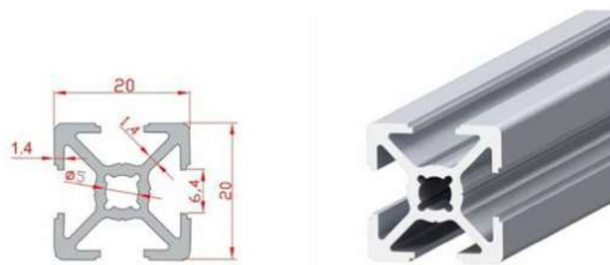


Fig. 4 Sigma profiles used in our study

motor by integrating the screw shaft into the hole under it. We printed this panel with a 3D printer and integrated it into our system. The carrier panel design is shown in Fig. 6.

The final structure of the updated plasma arc device, including the frame of the device, linear rail guides, and integrated step motor for microchannel operation, is shown in Fig. 7.

Fig. 5 Step motor and its circuit schema [26]

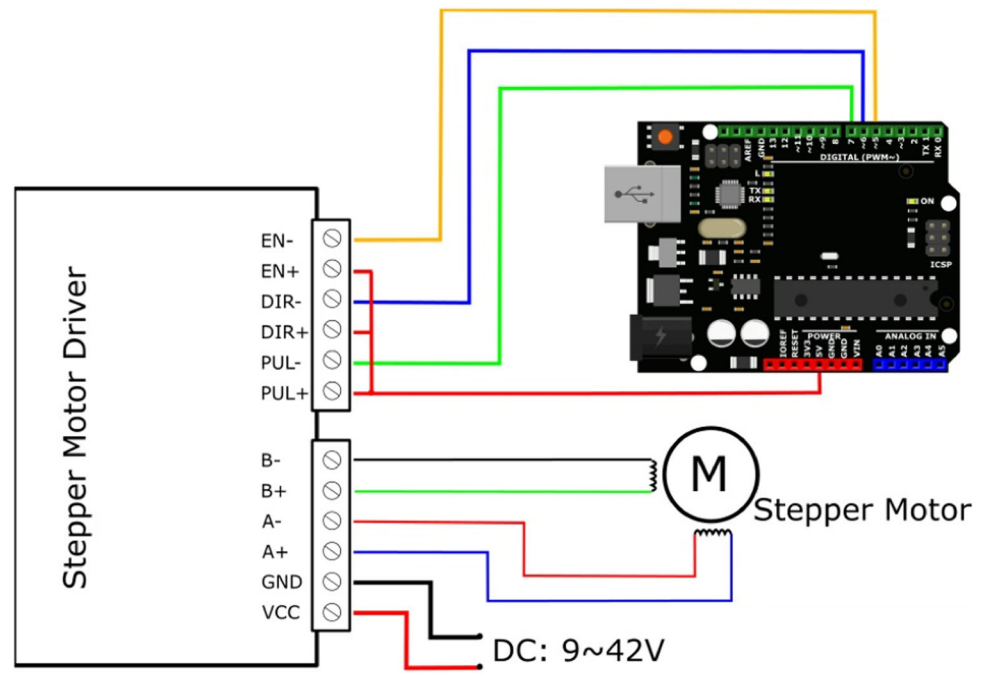


Fig. 6 Updated panel design



Fig. 8 Microchannel processing operation

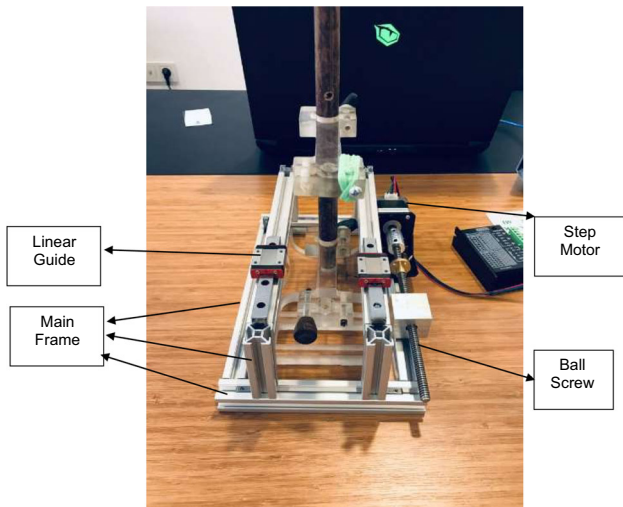


Fig. 7 Updated plasma arc device's main frame

3 Microchannel Processing

Probes do not move in the plasma arc device. Therefore, we drilled the board that held the probes fixed and screwed in there. We added an apparatus to the end to hold the glass. Thus, when we turned the screw, it was moved on the glass, and a microchannel was created by finding the appropriate distance between the probes and the appropriate glass thickness (1 mm) (Fig. 8).

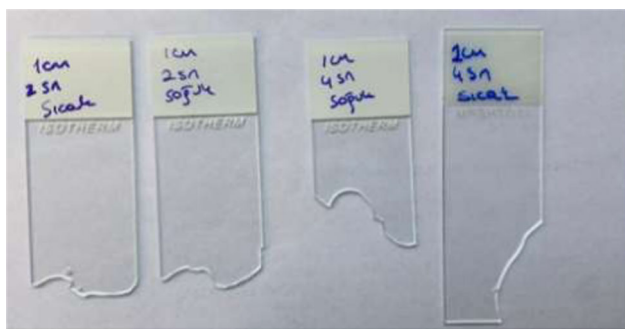


Fig. 9 Trial 1: unsuccessful

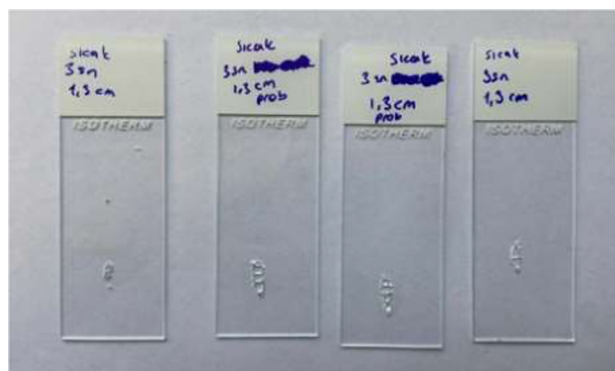


Fig. 11 Trial 3: successful

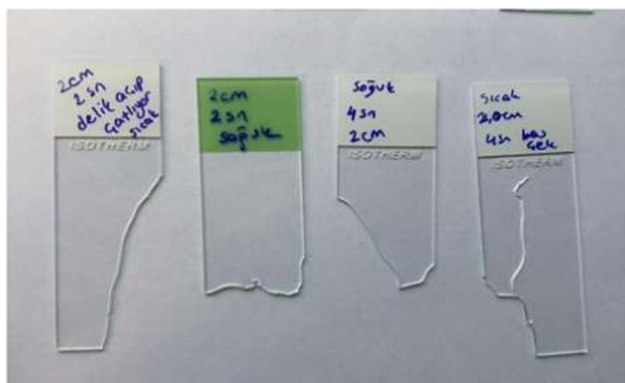


Fig. 10 Trial 2: unsuccessful

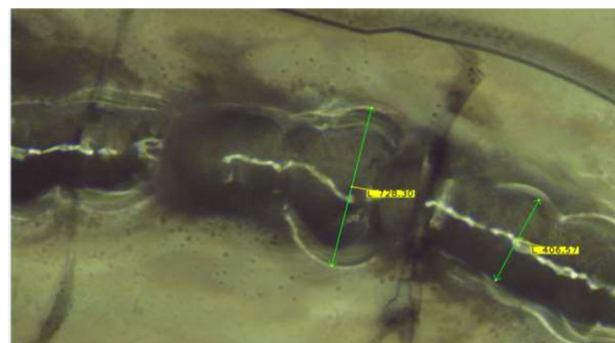


Fig. 12 Microchannel wicks

3.1 Experimental Design

The most effective experimental design method is the factorial design, which includes the effects of measurable factors and has the smallest error. In the factorial design, both the main effects of the factors and the interaction effects can be estimated. Factorial experiments or, as stated in many sources, factorial designs are very popular designs used to simultaneously investigate the main effects and interaction effects of two or more factors. There are three factors, each with two levels, to be changed in the experiments.

$$x = n^k \tag{1}$$

where x represents the factorial design, n represents the number of factor levels, and k represents the number of factors.

3.2 Preliminary Trials

As a result of the preliminary trials shown in Figs. 9, 10 and 11, we determined that our factors were the distance between probes, duration, and material temperature.

Distance between probes: The arms holding the probes in the plasma arc device were adjusted manually. The distance between the probes is crucial for the plasma power density

and plasma spot density [27, 28]. These factors impact the quality of the microchannel. Therefore, we tested several distance options, as shown in Fig. 11. As a result of the trials that we performed, it was observed that a suitable distance could be 1.3 cm based on the appropriate operation conditions of the plasma arc device, according to Trial 3 in Fig. 11.

Duration: During the production of microchannels, the heat of the plasma arc is not overloaded by the material being operated on, so the device only works for a certain period of time and is restarted after waiting for that time. As a result of the preliminary experiments, the appropriate processing time for the microchannels created was determined to be 3 s. As a result, a smooth microchannel image was obtained (Fig. 12). When the same process was used for 2 and 4 s, the desired result could not be obtained on the glass.

Temperature: To heat the coverslips, the glass slides were kept in a 35 °C container for 2 min. To determine whether the temperature was a factor, experiments were carried out with glasses heated at 35 °C for 2 min and with glasses kept at room temperature.

Frequency and Power: These are fixed factors since the optimal values determined in the initial design of the device are used.

As a result of these preliminary tests, we determined the lower and upper limits of our factors, as shown in Table 2.

Table 2 Factors and their levels

Factors	Level 1	Level 2
Distance between probes (A)	1 cm	1.3 cm
Duration (B)	2.5 s	3.5 s
Material temperature (C)	20 °C	70 °C

Table 3 Experimental design and response values

Experiments	Factors and their levels			Response (Delamination)
	A	B	C	Y (D_f)
1	1.0	3.5	20	1.64
2	1.3	2.5	70	1.60
3	1.0	2.5	70	1.32
4	1.0	2.5	20	1.20
5	1.3	2.5	20	1.62
6	1.3	3.5	20	1.75
7	1.3	3.5	70	1.95
8	1.0	3.5	70	1.72

The experimental design was subsequently created ($2^3 = 8$) (Table 3).

3.3 Response

The response is determined as delamination. Laminated materials are the most common type of damage due to the low strength between the layers. Delamination tends to degrade the strength and durability of a coating as well as the esthetic appearance of the material. The delamination coefficient is calculated as follows:

$$D_f = D_{max}/D_{min} \quad (2)$$

where D_f represents the delamination value, D_{max} represents the largest channel width, and D_{min} represents the narrowest channel width on the line.

3.4 Measurement Process

To measure the holes formed in the experiments according to the test matrix, help was taken from a Nikon Eclipse MA100 microscope (LE Plan 5X/0.10 ∞ /0 WD31) and Clemex Captiva software (Fig. 12).

4 Model Solution and Validation

The p-value is a measure of probability for the evidence against the null hypothesis (H_0). The H_0 provides evidence that the factor effects. Lower values for probability measures present stronger evidence against the H_0 . The p-value is used in the ANOVA table to obtain whether factor effects are statistically significant. A significance level (α) of 0.05 is usually chosen and works well in analyses. If $p \leq 0.05$, we reject the H_0 and conclude that all evaluated means are not equal. We can use our knowledge to obtain whether the effects are significant in interpreting the result. If $p > 0.05$, it means that we do not have enough evidence to reject the H_0 that the population means are all equal. We must clarify that our test result has sufficient power to obtain a practically meaningful difference.

The ANOVA table was constructed from the MINITAB data, as shown in Table 4. According to Tables 4 and 5, factors A (distance between probes) and B (duration) are efficient factors in the response since the p values are 0.03 and 0.019, respectively ($p < 0.05$ for 95% confidence level).

However, C (material temperature) is not an effective factor in the response since its p-value (0.175) is greater than 0.05. Additionally, the A*B and B*C interactions are not effective for Y because their p values are greater than 0.05. This situation is also shown in Table 5. Two-way interactions did not affect the response values. Its p-value (0.296) is greater than 0.05.

Interaction plots for Factors A, B, and C are shown in Fig. 13. As shown, there are no interactions between factors, and they are independent of each other.

The counterplots were analyzed in the present study. Figure 14 shows in detail the counterplots of factors A, B, and C. According to Fig. 14a, the minimum delamination yield obtained for A is less than 1.05, that obtained for B is less than 2.7, and that obtained for C is 20 (hold value for Fig. 14a). At these levels, the Y value is smaller than 1.3. On the other hand, for the highest values for A and B (1.3 and 3.5, respectively), the Y value is greater than 1.7. The minimum delamination yield obtained for A is less than 1.02, that obtained for C is less than 70, and that obtained for B is 2.5 (hold value for Fig. 14b) according to Fig. 14b. At these levels, the Y value is smaller than 1.3.

On the other hand, for the highest values for A and C (1.3 and above 40, respectively), the Y value is greater than 1.6. If the value of A increases from 1.00 to 1.05, the C value must be lower than 30 to reach $Y < 1.3$. A similar case is suitable for B and C. The best result for the response value ($Y < 1.3$) is obtained when B is smaller than 2.6, C is smaller than 70, and A is 1 (hold value for Fig. 14c).

The response optimizer tool runs with different target values for response to obtain the optimal factor values (Fig. 15). Factors A and C are held constant for all the cases when A =

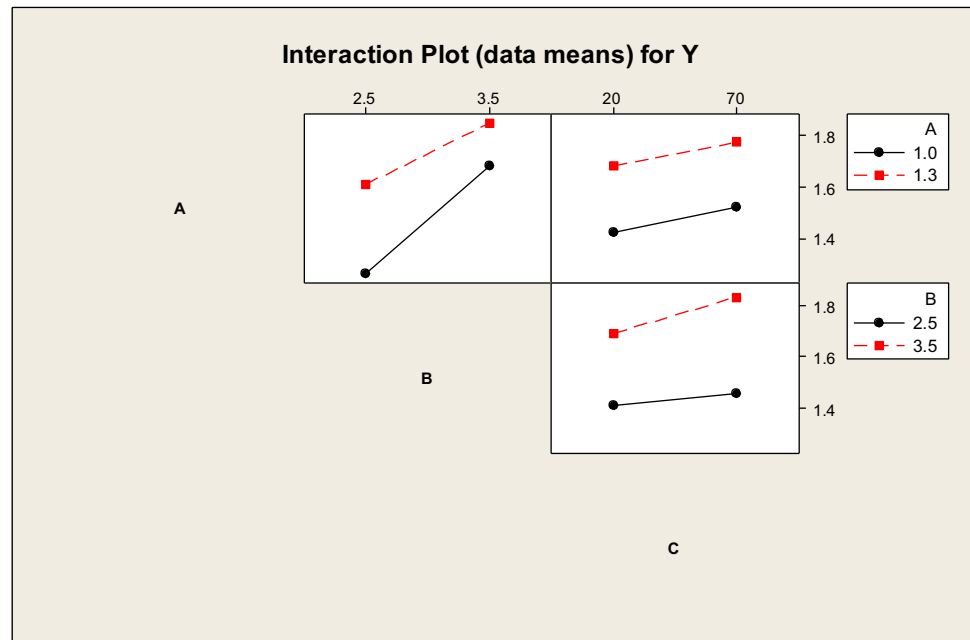
Table 4 Estimated effects and coefficients for Y (coded units)

Term	Effect	Coef	SE coef	T	P
Constant		1.60000	0.02305	69.42	0.000
A	0.26000	0.13000	0.02305	5.64	0.030
B	0.33000	0.16500	0.02305	7.16	0.019
C	0.09500	0.04750	0.02305	2.06	0.175
A*B	− 0.09000	− 0.04500	0.02305	− 1.95	0.190
B*C	0.04500	0.02250	0.02305	0.98	0.432
S = 0.0651920		R-Sq = 97.87%		R-Sq(adj) = 92.56%	

Table 5 Analysis of variance for Y (coded units)

Source	DF	Seq SS	Adj SS	Adj MS	F	P
Main effects	3	0.371050	0.371050	0.123683	29.10	0.033
2-way interactions	2	0.020250	0.020250	0.010125	2.38	0.296
Residual error	2	0.008500	0.008500	0.004250		
Total	7	0.399800				

Fig. 13 Interaction plots for Y



1 cm and C = 20 °C. However, factor B changes for different target values. As a result of the optimization study, the optimal factor levels are A = 1 cm, B = 2.5 s, and C = 20 °C. On the other hand, B can be set between 2.5 s and 2.54 s. This range is very restricted by factor B (Fig. 16). When the B value increases from 2.5 s to 2.94 s, the Y value dramatically increases from 1.235 to 1.4.

4.1 Confirmation Tests

We performed a confirmation test using the optimal parameter values (Fig. 17). We conducted three replications with

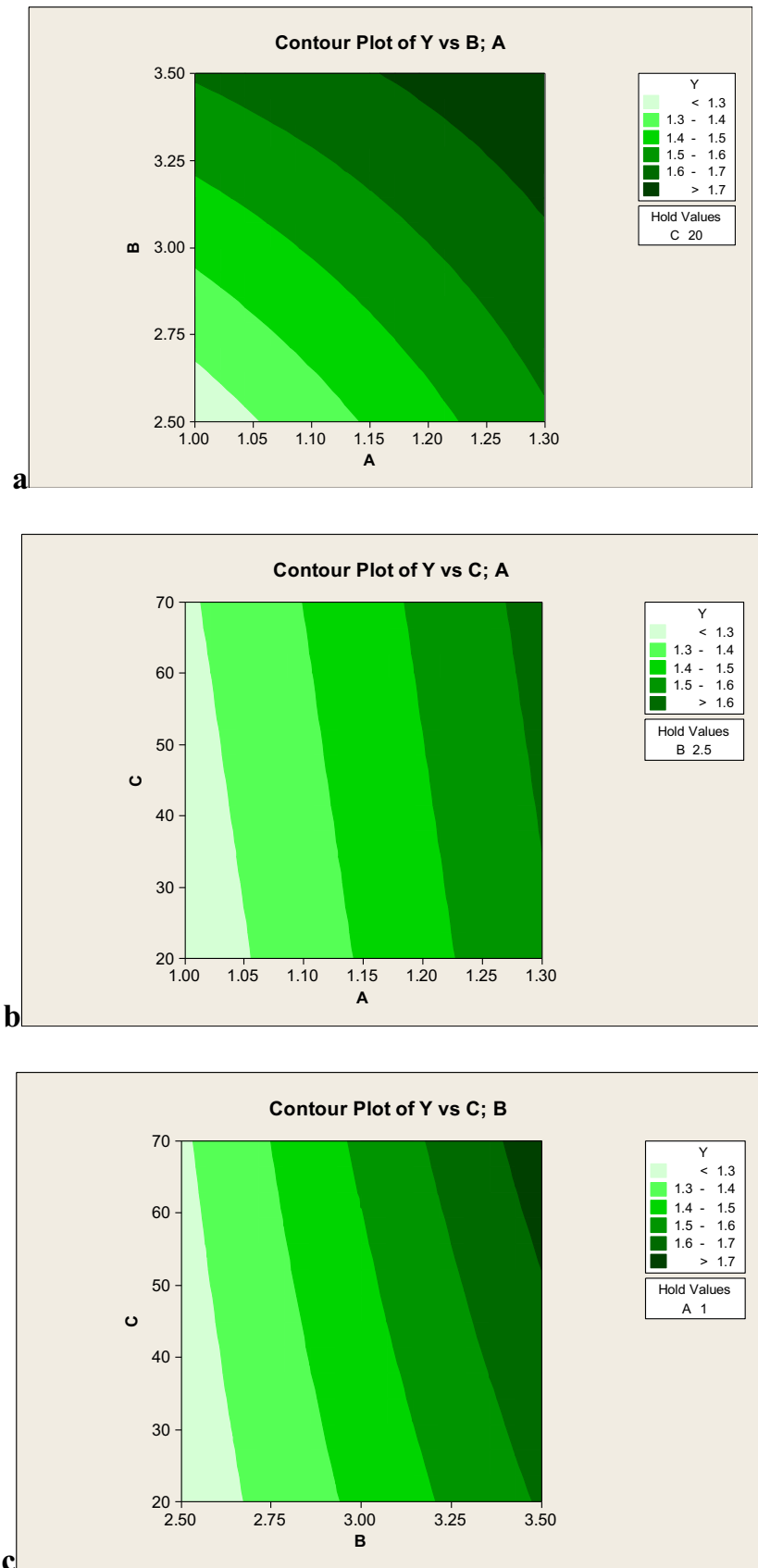
the optimum parameter values and collected response values for delamination as follows:

- Test 1: 1019/853 = 1.195,
- Test 2: 1293/1072 = 1.206,
- Test 3: 1493/1102 = 1.355,
- Average: 1.252.

As a result of the confirmation test (Table 6), we obtained a smoother microchannel using the optimal parameter values obtained with the developed plasma arc device.

Table 6 shows the confirmation test results for delamination under the predicted optimum factor levels. Table 6

Fig. 14 Contour plots for factors



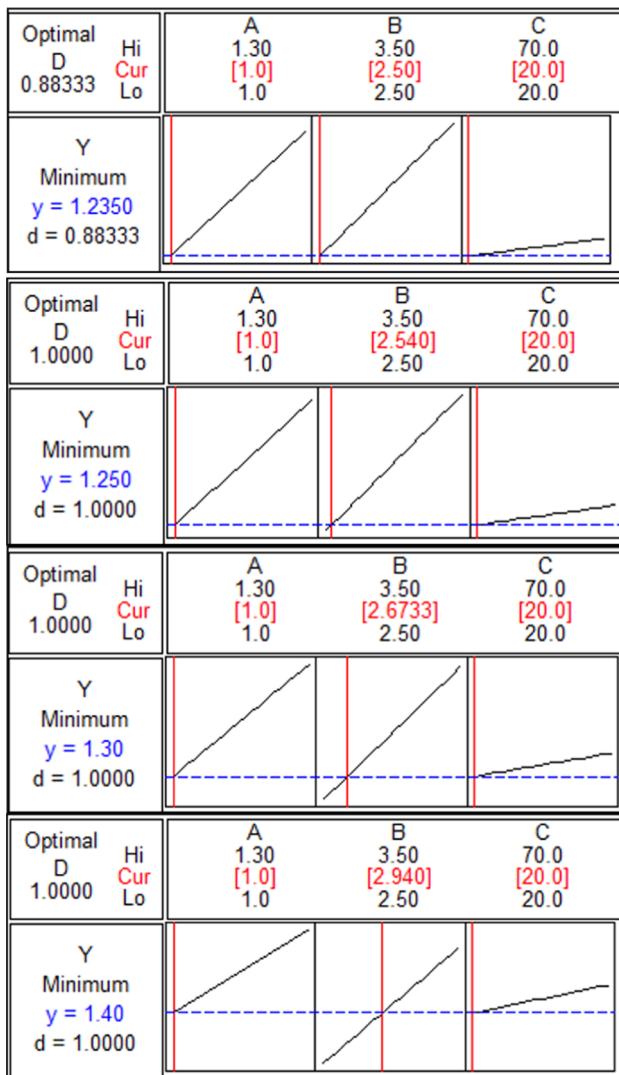


Fig. 15 Response optimization results

shows the closeness between the theoretical and experimental optimum values of D_f . The calculated error is less than 3.5343% for the optimum factor levels as shown in Table 6. The error among the experimental and optimization model results is very small, which affirms the experimental conclusion. Therefore, the analytical power of the proposed model is sufficient and suitable within the experimental domain.

4.2 Comparison with the Extant Literature

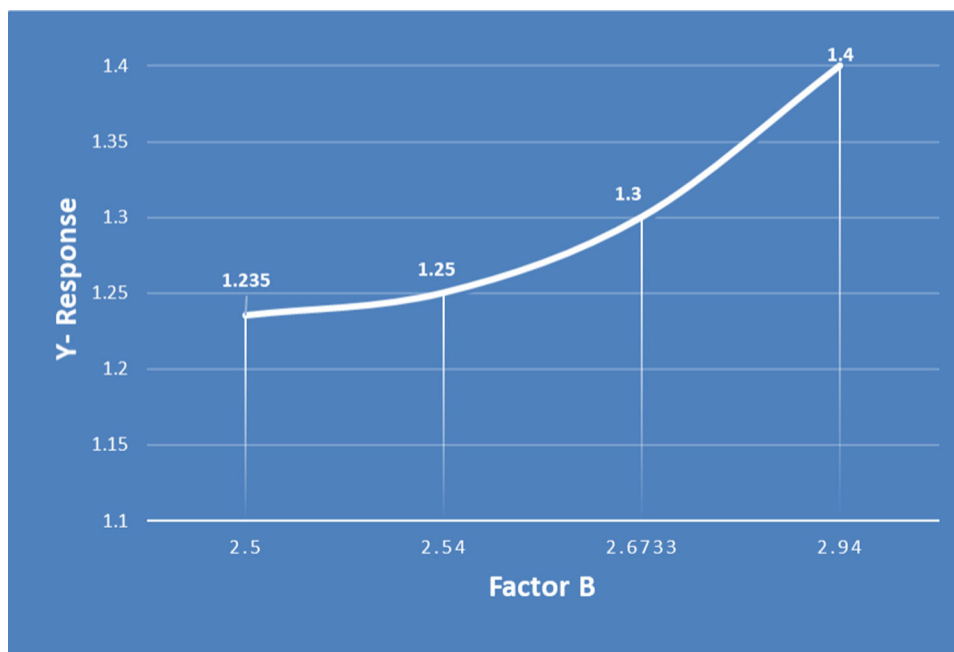
Sharma and Joshi [3] proposed a LIPAA (laser-induced plasma-assisted ablation) process for machining microchannels on transparent workpieces. They presented a two-dimensional transient numerical model to understand the physics of material removal during the LIPAA process. In their study, a thermophysical numerical model of the LIPAA based on the ablation of polycarbonate was developed.

The channel dimensions, i.e., the width and depth of the channel, were computed from the thermal distribution obtained from the numerical study. Overall, the authors concluded that the LIPAA process can be used to machine transparent workpieces such as polycarbonate and glass and that the proposed approach can be effectively used in the LIPAA process in practice. They used an L27 Taguchi design as an experimental design method. In their study, the best and worst values of the width were 561 and 246 μm , respectively. Therefore, their delamination value is 2.2805. Our best delamination value is 1.195 (the best value from the confirmation test). Therefore, our result is 47.55% more effective when considering the delamination value. Therefore, our results are competitive with the results obtained from the LIPAA process for transparent material microchannel fabrication using high-energy sources such as lasers or plasma. Although the processing capability of these materials is more difficult than that of polycarbonate materials, we successfully fabricated a microchannel on glass materials in this study.

5 Conclusions

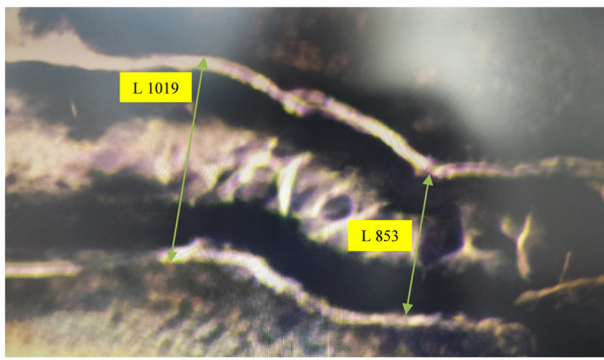
In this study, the cutting parameters that optimize the microchannel processing quality were determined with a current sensing plasma arc device. In addition, the mechanical design of the existing plasma arc device has been improved to obtain good quality with minimum channel width. As a result of these studies, microchannel fabrication can be performed successfully with minimum delamination. The distance between the probes and the duration parameters was effective for determining the channel quality. The optimization result obtained with the validation experiment was also confirmed.

Fig. 16 Optimization results against changing factor B values

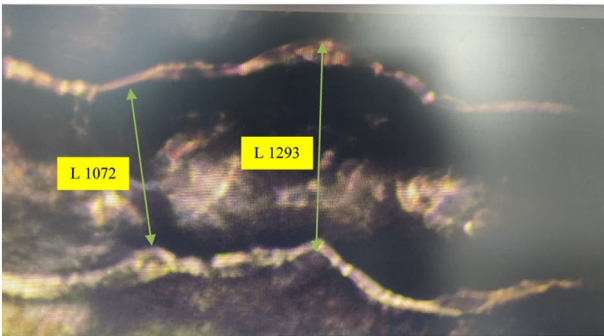


Based on the experimental results and analysis, the following conclusions can be drawn:

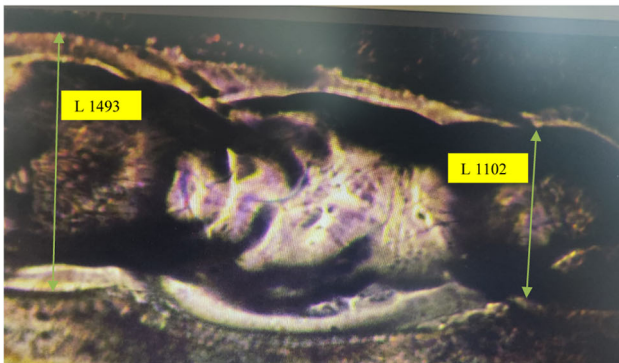
- (1) The minimum delamination is obtained for the smallest factor levels for A (distance between probes), B (duration), and C (material temperature). If the factor C is the highest value, B must be smaller than 2.54 s for minimum delamination when A is 1 cm.
- (2) A very similar condition is acceptable for A and C when B is constant at 2.5 s. If C increases from 20 °C to 70, A must be smaller than 1.05 cm.
- (3) If B increases from 2.5 s to 2.54 s when A is equal to 1 cm, C must be set at 20 °C for the smallest Y value.
- (4) The counterplots and optimization results show that new parameter ranges should be set for future investigations since A and C should be lower factor values for the optimal solution. The highest factor levels for A and C must be 1 cm and 20 °C, respectively, for future studies, and their lower values can be set as 0.5 cm and 150 °C, respectively.
- (5) The optimal factor values are $A = 1$ cm, $2.5 \text{ s} \leq B \leq 2.54$ s, and $C = 20$ °C.
- (6) The obtained results were confirmed via confirmation experiments with an error less than 3.5343%. The optimized result is an acceptable prediction of plasma arc-based microchannel processing parameters.
- (7) The narrow point angles of the tungsten electrodes could be as possible for dielectric discharge stability.
- (8) A chamber can be incorporated into the system, including argon, argon–hydrogen, and helium as the dielectric discharge-shielding gases.
- (9) Factor C can be set as 10–15 °C to make further investigation of the temperature effect.
- (10) For future work, a focus may be placed on performing narrower microchannel fabrication operations on different materials. The Pyrex or quartz materials can be used as work-piece material for material-specific process stability. The findings obtained in this study will constitute a reference for future studies.



Test 1



Test 2



Test 3

Fig. 17 Confirmation test results

Table 6 Confirmation test results

Initial parameter setting		Optimum parameter setting		Y (D _f)
A	B	C	Y (D _f)	
1.0	2.5	20	1.20	1.20
Optimum parameter setting				
1.0	2.5	20	1.195	1.195
1.0	2.54	20	1.206	1.206
1.0	2.94	20	1.355	1.355
Average result for confirmation test				
Average predicted result (Fig. 14)				
Predicted error				
Predicted error (%)				

Acknowledgements The basic version of the current detection plasma arc device used in this research has been patented by the Turkish Patent and Trademark Office (patent no: TR 2015 14159 B).

Author Contributions Fevzi Akın, Ece Ersoy, Deniz İdil, Melih Özsimiççi, and Kemal Okat wrote the manuscript draft and set the experimental environment and programmed the device. Dilek Çökeliler Serdaroğlu, Cengiz Koçum, Yusuf Tansel İç, and Kumru Didem Atalay developed the conceptualization, methodology, and writing-review and editing. All the authors reviewed the manuscript.

Funding Open access funding provided by the Scientific and Technological Research Council of Türkiye (TÜBİTAK).

Data Availability Not applicable.

Declarations

Competing interests Not applicable.

Ethical Approval Not applicable.

Open Access This article is licensed under a Creative Commons Attribution 4.0 International License, which permits use, sharing, adaptation, distribution and reproduction in any medium or format, as long as you give appropriate credit to the original author(s) and the source, provide a link to the Creative Commons licence, and indicate if changes were made. The images or other third party material in this article are included in the article's Creative Commons licence, unless indicated otherwise in a credit line to the material. If material is not included in the article's Creative Commons licence and your intended use is not permitted by statutory regulation or exceeds the permitted use, you will need to obtain permission directly from the copyright holder. To view a copy of this licence, visit <http://creativecommons.org/licenses/by/4.0/>.

References

- P. Chandra, E. Segal, (2016). Nanobiosensors for Personalized and Onsite Biomedical Diagnosis. The Institution of Engineering and Technology.
- Kim, K.R.; Kim, H.J.; Il Choi, H.; Shin, K.S.; Cho, S.H.; Choi, B.D.: Ultrafast laser microfabrication of a trapping device for colorectal cancer cells. *Microelectron. Eng.* **140**, 1–5 (2015)
- Sarma, U.; Joshi, S.N.: Spatial and temporal thermophysical analysis of Laser-induced plasma assisted ablation (LIPAA) of polycarbonate. *Opt. Laser Technol.* **150**, 107908 (2022)
- Li, G.; Xu, S.: Small diameter microchannel of PDMS and complex three-dimensional microchannel network. *Mater. Des.* **81**, 82–86 (2015)
- Nieto, D.; Delgado, T.; Flores-Arias, M.T.: Fabrication of microchannels on soda-lime glass substrates with a Nd:YVO4 laser. *Opt. Lasers Eng.* **63**, 11–18 (2014)
- Prakash, S.; Kumar, S.: Fabrication of rectangular cross-sectional microchannels on PMMA with a CO2 laser and underwater fabricated copper mask. *Opt. Laser Technol.* **94**, 180–192 (2017)
- Wu, T.; Ke, C.; Wang, Y.: Fabrication of trapezoidal cross-sectional microchannels on PMMA with a multipass translational method by CO2 laser. *Optik* **183**, 953–961 (2019)
- Groover, M.P.: *Fundamentals of modern manufacturing: materials, processes, and systems*. Wiley, Hoboken (2020)
- Kalpakjian, S.; Schmid, S. R. (2014). *Manufacturing processes for engineering materials–5th edition*. Agenda.
- DeGarmo, E.P.; Black, J.T.; Kohser, R.A.: *DeGarmo's materials and processes in engineering* (2007)
- Sen, M.; Shan, H.S.: A review of electrochemical macroto micro-hole drilling processes. *Int. J. Mach. Tools Manuf.* **45**(2), 137–152 (2005)
- Deli, J.; Bo, Y.: An intelligent control strategy for plasma arc cutting technology. *J. Manuf. Process.* **13**(1), 1–7 (2011)
- Sun, H.; Kusumoto, K.: Drilling performance of plasma arc drilling method. *Q. J. Jpn. Weld. Soc.* **28**(4), 421–426 (2010)
- Kusumoto, K.; Sun, H.; Ishikawa, S.: Observation of hole formation process in plasma arc drilling. *Q. J. Jpn. Weld. Soc.* **29**(3), 66s–70s (2011)
- Kusumoto, K.; Sun, H.: Development of drilling method using plasma arc technology. *Q. J. Jpn. Weld. Soc.* **28**(4), 415–420 (2010)
- Rathinasuriyan, C.; Chandar, J.B.; Palanisamy, R.: Optimization of roundness in plasma arc drilling process by Taguchi approach. *Mater. Today: Proc.* **52**, 278–282 (2022)
- Timoshkin, I. V.; Mackersie, J. W.; MacGregor, S. J. (2003, June). Plasma channel microhole drilling technology. In *Digest of Technical Papers. PPC-2003. 14th IEEE International Pulsed Power Conference (IEEE Cat. No. 03CH37472)* (Vol. 2, pp. 1336–1339). IEEE.
- Kozak, J.; Rajurkar, K.P.; Balkrishna, R.: Study of electrochemical jet machining process. *J. Manuf. Sci. Eng.* (1996). <https://doi.org/10.1115/12831058>
- Sharma, S.; Jain, V.K.; Shekhar, R.: Electrochemical drilling of inconel superalloy with acidified sodium chloride electrolyte. *Int. J. Adv. Manuf. Technol.* **19**(7), 492–500 (2002)
- Snoeys, R.; Staelens, F.; Dekeyser, W.: Current trends in nonconventional material removal processes. *CIRP Ann.* **35**(2), 467–480 (1986)
- Chamarthi, S.; Reddy, N.S.; Elipey, M.K.; Reddy, D.R.: Investigation analysis of plasma arc cutting parameters on the unevenness surface of Hardox-400 material. *Procedia Eng.* **64**, 854–861 (2013)
- Amalnik, M.S.; McGeough, J.A.: Intelligent concurrent manufacturability evaluation of design for electrochemical machining. *J. Mater. Process. Technol.* **61**(1–2), 130–139 (1996)
- Rajamani, D.; Ananthakumar, K.; Balasubramanian, E.; Paulo Davim, J.: Experimental investigation and optimization of PAC parameters on Monel 400™ superalloy. *Mater. Manuf. Process.* **33**(16), 1864–1873 (2018)
- Das, M.K.; Kumar, K.; Barman, T.K.; Sahoo, P.: Optimization of process parameters in plasma arc cutting of EN 31 steel based on MRR and multiple roughness characteristics using gray relational analysis. *Procedia Mater. Sci.* **5**, 1550–1559 (2014)
- Hong, B.; Qu, Y.; Hong, Y.; Li, M.; Zou, Y.: Modelling and optimising process of micro-plasma arc freeform fabrication. *Mater. Des.* **228**, 111854 (2023)
- Internet: <https://forum.arduino.cc/t/stepper-motor-cycle-time/569008>, Acces date: February 5, 2024.
- Kostov, K.G.; Nishime, T.M.C.; Castro, A.H.R.; Toth, A.; Hein, L.R.D.O.: Surface modification of polymeric materials by cold atmospheric plasma jet. *Appl. Surf. Sci.* **314**, 367–375 (2014)
- Do Nascimento, F.; Stancampiano, A.; Trebulová, K.; Dozias, S.; Hrudka, J.; Krčma, F.; Pouvesle, J.M.; Kostov, K.G.; Robert, E.: Plasma electrode dielectric barrier discharge development, characterization and preliminary assessment for large surface decontamination. *Plasma Chem. Plasma Process.* **43**(6), 1791–1817 (2023)

